

Measuring the neutron star equation of state from EMRIs in dark matter environments with LISA

Theophanes K. Karydas^{1,*} and Gianfranco Bertone¹

¹*Gravitation Astroparticle Physics Amsterdam (GRAPPA),
University of Amsterdam, 1098 XH Amsterdam, The Netherlands*

Gravitational-wave observations of extreme mass-ratio inspirals (EMRIs) in vacuum are largely insensitive to the internal structure of the small compact companion. We show that this conclusion can change when the central black hole is surrounded by a dense dark matter environment. We compute, for the first time, the relativistic dynamical-friction force on a neutron star moving through a collisionless medium and its impact on the evolution of EMRIs embedded in dense dark matter spikes. We then perform a Bayesian parameter-estimation analysis of simulated LISA observations to assess the measurability of both spike properties and the companion's internal structure. We find that, in our fiducial dark matter spike models, EMRIs with signal-to-noise ratio (SNR) $\gtrsim 20$ already allow us to distinguish neutron star from black hole companions, while events with SNR $\gtrsim 400$ make it possible to discriminate between different neutron star equations of state.

Introduction. With the advent of next-generation millihertz gravitational-wave (GW) detectors [1–3], it will become possible to monitor extreme mass ratio black hole (BH) binaries over long timescales. Such measurements will enable detailed investigations of the astrophysical environments where binaries form and evolve [4–12], opening a wide range of possibilities for fundamental physics. These range from stringent probes of gravity [13–16] to searches for new physics in the particle sector [17–22]. A particularly compelling scenario involves dark matter (DM) overdensities, or *spikes*, around BHs [23–29], which can influence the orbital evolution of inspiraling binaries [30–49].

The interaction of EMRIs with standard non-interacting particle DM is mediated only by gravity. The leading environmental effects in this case arise from dynamical friction [50–52] and, for BH companions, from particle accretion [34, 49, 53, 54]. Both effects are sensitive to the internal degrees of freedom of the small companion object, such as its mass and spin [55–58].

Neutron stars (NS) are extremely compact astrophysical objects [59–61], and their interior provides a unique laboratory for the equation of state (EOS) of strongly interacting matter at supranuclear densities [62], where exotic degrees of freedom [63–66] or phase transitions [67] may occur. Probing this regime is one of the central goals of multi-messenger astronomy [68–70]. Thus far, the detections of comparable mass ratio compact binaries by the LVK [71–73] collaboration have yielded constraints on NS properties [74–80], offering direct empirical insight into the behavior of dense matter. In sharp contrast, GWs from EMRIs in vacuum (with mass ratio, $m/M \leq 10^{-5}$) are often argued to be insensitive to the nature of the companion [81].

Here, we demonstrate that environmental effects from DM can render EMRI waveforms sensitive to the nature of the small compact object. Specifically,

we study the impact of a DM spike on the GW emission of an EMRI consisting of a NS orbiting a supermassive BH. We show that for our fiducial spike models (i), the spike parameters can be accurately recovered already for any detectable waveform, largely irrespective of the nature of the companion, and (ii) for sufficiently high SNR, the nature of the companion can be distinguished: SNR $\gtrsim 20$ enables discrimination between certain NS models and BH secondaries, while SNR $\gtrsim 400$ yields sensitivity to differences among all tested NS equations of state.

Setup. We consider an EMRI in which a NS orbits a massive BH embedded in a dark matter DM spike. As the companion moves through the surrounding DM distribution, dynamical friction provides an additional dissipative channel that alters the orbital evolution [30, 31]. To model the inspiral, we adopt the adiabatic framework, in which the EMRI is described as a slow secular drift through a sequence of bound geodesics of the background BH spacetime [82, 83].

At leading order, the secular evolution is governed by the orbit-averaged fluxes of energy, angular momentum, and Carter's constant [53, 84]. In this work, we study quasi-circular inspirals around a non-spinning BH where due to symmetry inspirals are characterized only by the flux for angular momentum loss. Under these assumptions, and when at separation r , the rate of change of the NS's angular momentum L is

$$\frac{dL}{dt} = rF_\phi \frac{\sqrt{1 - 2GM/(c^2r)}}{1 - 3GM/(c^2r)}, \quad (1)$$

where the fraction is a strong field correction (at most a $\sim 6\%$ enhancement at the innermost stable circular orbit with respect to the non-relativistic case, $\dot{L} = rF_\phi$) and F_ϕ is the dynamical friction force acting on the NS in the direction of its motion which we compute below. This flux will then be incorporated within the `FastEMRIWaveforms_v2.0.0` (FEW) framework [85–88] to generate highly accurate GW waveforms.

* t.karydas@uva.nl

Dynamical friction on neutron stars. Dynamical friction is the dominant mechanism through which compact objects exchange momentum with their surrounding medium in collisionless environments such as cold DM spikes [50–52]. While Newtonian prescriptions exist for both point masses and extended perturbers [89–91], and relativistic formulations have been developed for BHs [53, 54], NSs cannot be fully captured by either framework. This is because they possess a finite size, EOS-dependent density profiles, and an extreme compactness which makes it impossible to neglect strong-gravity effects in their vicinity. To address this, we develop a relativistic framework for computing dynamical friction on NSs. In absence of a dissipative coupling between baryonic and dark matter, the force experienced by NS is given by

$$\mathbf{F} = \int \gamma \mu f(\mathbf{v}) v \sigma_{\text{scatter}}(v) \mathbf{v} d^3\mathbf{v}, \quad (2)$$

where \mathbf{v} is the relative velocity of the particles sampled from the distribution function $f(\mathbf{v})$ [26, 92] in the NS’s frame of reference, γ is the Lorentz factor, and μ is the particles’ rest mass. The term σ_{scatter} represents the cross-section for exchange of momentum via gravitational scattering. For spherically symmetric interactions (cf. discussions), it is

$$\sigma_{\text{scatter}} = 4\pi \int_0^{b_{\text{max}}} b \cos^2 \chi db, \quad (3)$$

where $b_{\text{max}} = r(q/3)^{1/3}$ is the Hill radius, and χ is the azimuthal difference in the position of a particle between infinity and the point of closest approach. It is related to the deflection angle through $\theta_{\text{defl}} = 2\chi - \pi$ (cf. [92, Fig. 3.2]). Evaluating Eq. (3) requires solving the geodesic equations governing particle motion in the NS spacetime whose computation is discussed in Section A.

To assess the impact of the DM environment on the companion’s orbit, we numerically integrate Eq. (3) for the NS spacetime and insert it into Eq. (2) and Eq. (1), which are themselves integrated over the spike’s velocity distribution. In Section B we give present the technical details of the calculation. We assume the relativistic distribution function from Ref. [26], derived for the adiabatic growth of a non-spinning BH, and transform it to the NS frame, accounting for the central BH’s strong gravity as in [48]. To capture a representative range of possible NS structures, we consider three EOS highlighted in [93] for being compatible with with tidal deformability constraints from GWs [78] and heavy pulsar observations [94]: MPA1 [95], AP3 [96] and SLy [97], which are matched with a crust as in [98]. The EOS and resulting radial profiles of the change in friction are shown in Fig. 6 alongside a collection of other representative models.

In Fig. 1, we show the drag force F (normalised by q^2 so that the BH curve is approximately constant) as a function of the companion mass. The behaviour of the NS curves can be understood as follows.

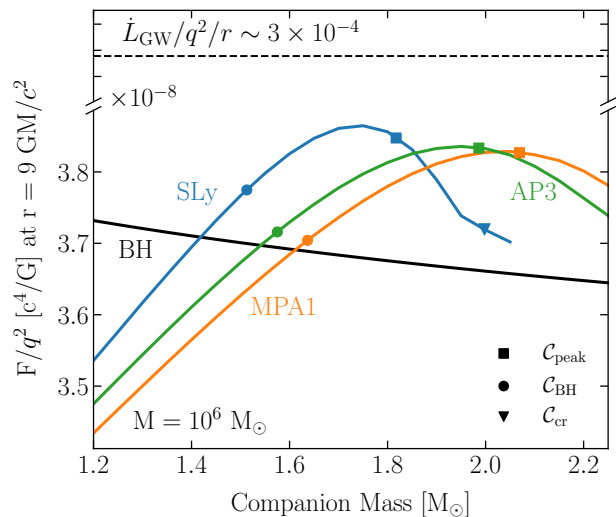


FIG. 1. **Dynamical friction as a function of companion mass.** Markers indicate the predicted onset of key features from a constant-density-sphere toy model for $u = \langle u \rangle_{9GM/c^2}$. A NS’s crust causes the toy model to overestimate the true values, particularly for SLy’s thick crust.

- At low masses, the drag on NSs is weaker than for BHs due to their smaller compactness, which effectively dilutes the density probed by DM orbits and yields a smaller dynamical friction force than BH accretion.
- As the mass (and hence the compactness) increases, the NS drag overtakes the BH value: this is a genuinely relativistic effect driven by nearly radial encounters that would have been accreted by a BH but are instead strongly deflected by the NS. Particles scattered through an obtuse angle transfer more momentum to the star than accretion would (cf. [92, Ch. 3]); in the extreme case of a $\sim 180^\circ$ deflection, the momentum transfer is equivalent to accreting two particles, effectively enhancing the cross-section.
- For even larger masses, the force reaches a maximum and then decreases, because the higher compactness allows particles to wind around the star and exit with acute scattering angles, which are less efficient at transferring momentum and thus reduce the scattering cross-section.

In Section C, we introduce an analytical toy model that reproduces this qualitative behaviour, and we use a constant-density sphere to estimate the compactness values at which the onset and peak of the enhancement occur.

Finally, while low-compactness stars may allow particles to graze their surface and smoothly reach deeper with decreasing impact parameter, sufficiently compact objects prohibit such grazing trajectories. In this case, radial encounters with $b < b_{\text{cr}}$ penetrate

the interior whilst effectively on a plunging trajectory, and reach discontinuously deep within the star before escaping due to the decrease in enclosed mass at the core. These will wind discontinuously more compared to slightly less radial encounters, thus changing the scattering cross-section for those compact objects. This effect arises as a generalization to the photon-sphere to account beyond just photons but particles moving with any velocity. Amongst our selected models, this only affects SLy which achieves the appropriate compactness.

Parameter estimation with incorrect models.

Having established the physical setup and the modeling framework for computing NS inspirals within DM spikes, we now turn to assessing the observability of these effects through future GW observations in the mHz band such as with LISA [5]. In particular, we first explore how parameter estimation is affected when the analysis is carried out with an incorrect model for the companion, and quantify the resulting biases in the inferred system parameters.

We quantify these biases using the Bayesian framework described in Section D. Specifically, we inject a waveform with a duration of 4 years, emitted by a binary with a NS companion described by the SLy equation of state and the intrinsic parameters of a benchmark system ($M = 10^6 M_\odot$, $m = 2 M_\odot$, and $\rho = 10 \rho_{\text{MW}} \approx 10^{18} M_\odot/\text{pc}^3$ at 10^{-6} pc, where ρ_{MW} represents the expected density for a Milky Way-like galaxy [23]) and then recover it using the true model or three alternative companion models: MPA1, AP3, and a BH. We adopt an SNR of 300 as a fiducial value, representing an optimistic scenario in which a single such event is detected during LISA's nominal four-year mission, obtained by rescaling the SNRs of Ref. [99] to NS companions. We emphasise, however, that EMRI rate predictions span nearly three orders of magnitude [99–101], and that estimates for systems with NS secondaries have so far been carried out only for in-situ formation channels [102]. The density and SNR choices adopted here should therefore be regarded as convenient benchmarks, rather than forecasts. The scaling of our results with these parameters is discussed in the next section.

In Fig. 2 we show the resulting one- and two-dimensional marginal posteriors, illustrating how the choice of companion model affects parameter recovery. We find that the component masses and DM spike normalization are recovered with similar accuracy across all companion models, with only a modest bias when an incorrect model is used. In particular, the $\sim 5\%$ bias in the inferred DM density, shows that spikes remain clearly identifiable even when the companion assumption is incorrect, which highlights the potential of LISA to probe DM spikes.

Inferring the equation of state. We now turn to the prospects for inferring the NS EOS from GW observations of EMRIs in DM spikes. For each of the three NS

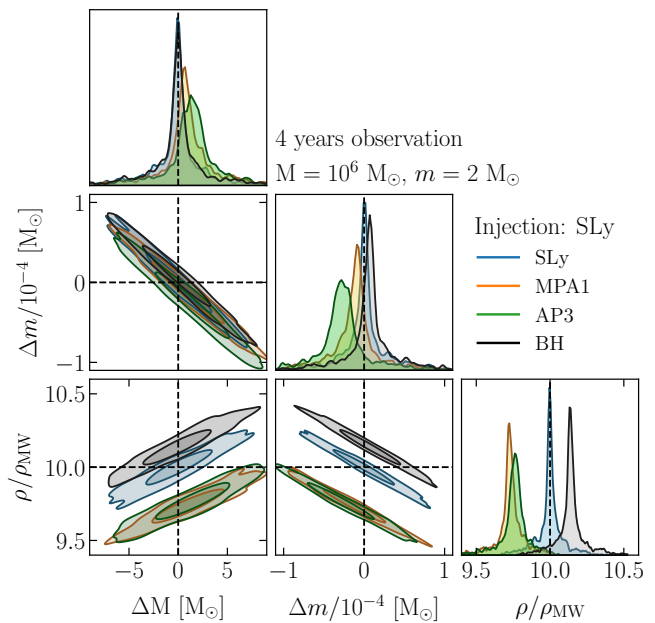


FIG. 2. **Marginal posteriors for the masses and spike density.** Results are based on 4 years of observation data, with black dashed lines indicating the injected values.

models (SLy, MPA1, AP3), we generate mock data sets containing an EMRI signal that includes the contribution of dynamical friction, and analyse each injection under four companion hypotheses: SLy, MPA1, AP3, and a BH. For every case, we compute the Bayesian evidence and construct Bayes factors, providing a quantitative measure of how strongly the data support each model. This allows us to assess whether the different companion models can be distinguished across the NS mass spectrum.

The results of this analysis are summarised in Fig. 3, which shows the Bayes factors \mathcal{B} for comparisons between different companion models across the range of NS masses considered. Most comparisons yield strong evidence ($\mathcal{B} > 10$) in favour of the true model, although some pairs provide less than substantial support ($\mathcal{B} < 3.2$), primarily for MPA1 versus AP3, which produce very similar NSs. In a subset of cases the Bayes factors reach the regime of decisive evidence ($\mathcal{B} > 100$). This is remarkable given that the EOS models we consider are already relatively similar, and all remain compatible with current tidal-deformability constraints from GW observations of binary NS mergers [78]. This highlights how DM environmental effects may allow us to probe the internal structure of the compact companion.

The mass dependence of the Bayes factors exhibits a correlation with the mass trends shown in Fig. 1. In particular, we observe that the Bayes factors disfavoring a model, for example, a BH, tend to reach their largest (or smallest) values at specific masses, consistent with the distance between forces from those models. We note that the curves shown in the figures are expected to shift toward slightly higher masses for snapshots at smaller radii, due to the increase in average particle velocity.

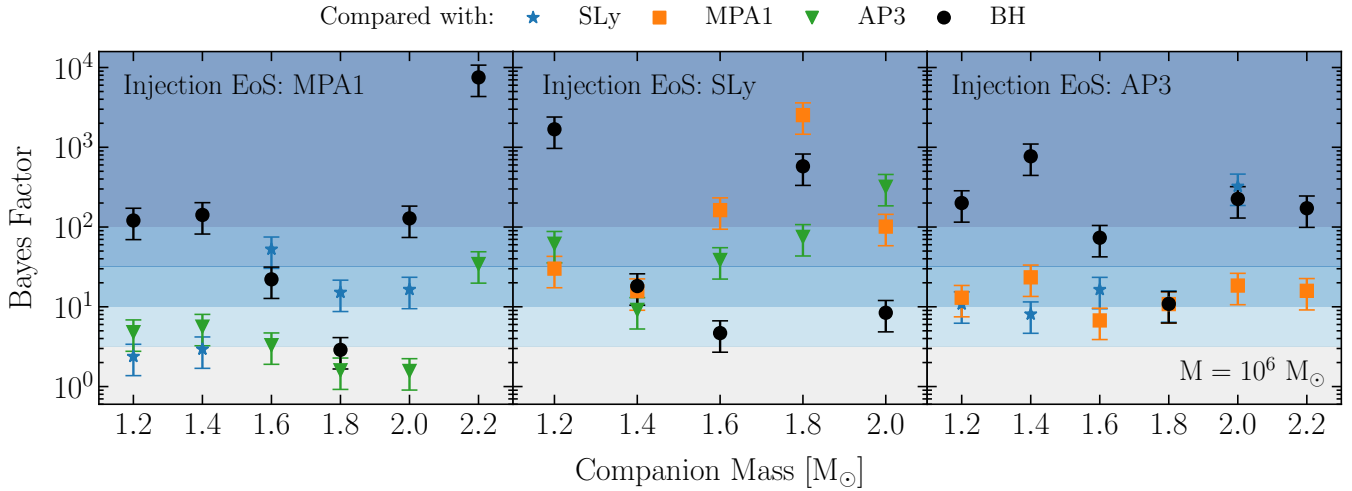


FIG. 3. **Bayes factors for EOS comparisons with different companion masses.** Colored bands denote the Jeffreys-scale interpretation [103] from “Trivial” (gray), to “Substantial”, “Strong”, “Very Strong”, and “Decisive” (dark blue). Error bars show the nested-sampling evidence uncertainty. The SLy EOS cannot achieve a $2.2 M_{\odot}$ configuration and is hence omitted.

Nevertheless, the shift is small, and the behavior at $r = 9 \text{ GM}/c^2$ provides a particularly useful diagnostic, as the majority of the inspiral’s impact is accumulated at larger separations and that radius approximately corresponds to the furthest distance over the 4-year span of waveform data.

Systems of interest. So far, we have demonstrated that the internal structure of the companion can be distinguished in a high-SNR EMRI embedded in a DM environment. We now turn to the conditions under which this effect remains detectable as we vary the system parameters. To this end, we use the Laplace approximation to the Bayesian evidence (cf. Section D) to make the exploration of parameter space computationally tractable. In Fig. 4, we illustrate how the discriminating power depends jointly on the SNR, the DM density, and the primary mass.

In this figure, the lines show the combinations of DM density and SNR for which the Bayes factor between the relevant models reaches the threshold for decisive evidence, $\mathcal{B} = 100$. Reading the plot from low to high density or SNR, four regimes emerge. At low density/low SNR, the DM-induced dephasing remains indistinguishable from a vacuum EMRI. For larger SNR, the presence of a spike can be established with decisive evidence once $\text{SNR} \gtrsim 400$ (20) for a $10^6 M_{\odot}$ ($10^5 M_{\odot}$) primary, while the companion models remain degenerate. At higher SNR, $\text{SNR} \gtrsim 800$ (400), subsets of EOS models yield $\mathcal{B} \geq 100$, and in the highest-density/highest-SNR regime all of our EOS comparisons satisfy the same decisive-evidence criterion.

We have chosen the primary mass to be $10^6 M_{\odot}$ (solid) or $10^5 M_{\odot}$ (dashed lines) to encompass the peak of the EMRI rate distribution [99, 101]; for reference, each case is normalized with the appropriate density to either the DM density expected for the Milky Way [23] ρ_{MW} , or

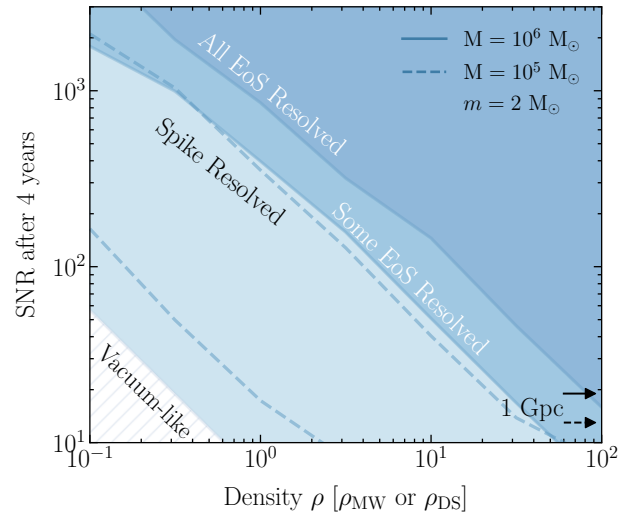


FIG. 4. **Minimum optimal signal-to-noise ratio accumulated after 4 years for distinguishing EMRIs with neutron star companions.** Arrows point the SNR for binaries placed at 1 Gpc distance. The vacuum-like region for the $10^5 M_{\odot}$ case lies outside the plot.

for Draco dSph [104] ρ_{DS} , respectively. Evidently, whilst the best-case region, where all EOS are resolved, is of the same size for both primary masses, the secondary region where only some can be resolved, is wider for the system with a lighter primary. This occurs because a larger mass ratio allows the companion to inspiral from larger initial separations (in terms of the primary’s gravitational radius) while still merging within a fixed time. As a result, the inspiral covers a wider portion of the dynamical friction profile, making features like changes in slope easier to measure. Repeating the analysis using waveforms with a shorter duration would restrict the regions and push the boundaries towards higher values of SNR.

Discussion. Although our discussion has centered on dynamical friction for compact objects in EMRIs, the framework applies equally to less asymmetric binaries, or isolated objects embedded in DM distributions. It can be readily extended to NSs described by different EOS than those investigated here, and generally to compact objects whose interior metric can be specified either from first principles, through an EOS, or a parametrized density profile. For instance, it can be applied to known astrophysical objects, like main sequence stars ($\mathcal{C} \sim 10^{-6}$) or white dwarfs ($\mathcal{C} \sim 10^{-3}$) within environments with relativistic velocity distributions. It can also be applied to exotic compact objects like strange quark stars, composed of deconfined strange quark matter [105, 106] which are generally more compact than ordinary NS; or boson stars [107], which could form from ultralight or self-interacting scalar fields [108]. Additional targets can be horizonless BH mimickers (cf. [109] and references therein), gravastars [110], or Q-balls [111], and even BHs with small environments around them, such as gravitational atoms [112] formed when ultra-light bosonic fields grow through superradiance [113], though one must adapt the formalism beyond spherical symmetry for most atom configurations.

Although our most striking result is the possibility of probing the internal structure of the compact companion, the region of parameter space in which LISA can distinguish NS from BH companions is also informative. The detection of unusually low-mass BHs, in particular, would point to nonstandard formation channels: they could, for instance, be primordial BHs [114, 115], or BHs formed through the DM-induced collapse of NSs. DM-nucleon interactions can, in fact, lead to accumulation of DM inside a NS. If the captured DM becomes self-gravitating and collapses to form a BH, the latter can grow by accreting nuclear matter and eventually consume the star from the inside (see, e.g., Refs. [116, 117]).

Accounting for DM-nucleon interactions, if present, in the complementary regime in which the DM mass and cross section do not trigger collapse over the NS lifetime, would require adapting the deflection formalism to include nuclear scattering. The extreme case where all particles crossing the interior are captured, the dynamical friction induced by a NS would be analogous to that induced by a BH, but with a larger geometric cross-section. We find that for a low NS compactness ($\mathcal{C} \sim 0.1$) it can be at most $\sim 50\%$. Therefore, realistic couplings¹ would only provide a subdominant contribution to the dynamical-friction force, highlighting the robustness of our analysis against possible DM-nucleon couplings.

Finally, we have neglected the spin of the NS, as its inclusion would affect our results only at higher order. Spin modifies the stellar structure [119, 120] and, at sufficiently rapid rotation, leads to mass shedding [121]; it also alters the exterior space-time from Schwarzschild but to a less pronounced extent compared to Kerr for the same spin [119, 122, 123]. Kerr BHs can therefore be used to obtain an upper bound on spin-induced modifications to dynamical friction. The effect scales as \tilde{a}^2 of the dimensionless spin, $\tilde{a} = cJ/Gm^2$ rather than only with angular momentum J , and changes at most by $\sim 10\%$ for an extremal BH, $\tilde{a} \sim 1$, (cf. [49, 55, 57]), whereas physically motivated EOSs yield NS spins no larger than $\tilde{a} \simeq 0.7$ [122]. Furthermore, isolated NSs at birth typically have $\tilde{a} < 0.04$, and accretion can increase their spin only up to $\tilde{a} \lesssim 0.4$ [124, 125], consistent with the fastest-rotating observed pulsar J1748-2446ad [126]. In fact, fewer than 1% of NSs are observed to exceed $\tilde{a} > 0.05$ [127]. To incorporate spin, the scattering framework would need to be extended following [128], but applied to the spacetime sourced by a rotating NS, and its structure needs to be modified accordingly.

Conclusions. In this work, we have shown that DM overdensities around BHs, such as DM spikes or mounds around massive BHs [23, 26–28], can render EMRI waveforms sensitive to the nature of the small compact object. In particular, we have explored the potential to probe NS internal structure and their equation of state [59–61] through EMRIs embedded within DM spikes observed by LISA [1].

We developed a relativistic framework for dynamical friction on compact objects moving through a collisionless medium, applicable to generic NS models with an arbitrary EOS as well as exotic compact objects, provided the internal metric is specified. Applying this framework to EMRIs with a NS secondary embedded in DM spikes, we computed the influence of the companion’s internal structure on the emitted gravitational waveforms using the FEW framework [85–88].

We find that, for our fiducial spike models, the binary masses and DM spike parameters can be accurately recovered for any detectable waveform, largely independently of the companion model. This implies that parameter estimation pipelines can be simplified without significant loss of precision. For sufficiently high signal-to-noise ratios, the additional friction induced by the companion’s internal structure becomes measurable. Using Bayesian model comparison, we have shown that such EMRIs can discriminate between BH and some NS companion models ($\text{SNR} \gtrsim 20$ if the primary is $\sim 10^5 M_\odot$, or $\text{SNR} \gtrsim 400$ if $\sim 10^6 M_\odot$) and, for louder events ($\text{SNR} \gtrsim 400$, or $\text{SNR} \gtrsim 800$ respectively), between any EOS tested (SLy, MPA1, AP3). These results highlight that LISA observations of EMRIs embedded in a DM environment could serve as a new astrophysical laboratory, probing both the distribution of dark matter around massive BHs and the microphysics of matter at supranuclear densities.

¹ Requiring the DM mean free path $\sim m_n/(\rho_{\text{nucleus}}\sigma_{\chi n})$, to exceed the NS radius so that particles undergo multiple scatterings before becoming gravitationally bound implies $\sigma_{\chi n} \gg 10^{-44} \text{ cm}^2$. Current limits already constrain $\sigma_{\chi n} \lesssim 10^{-41} \text{ cm}^2$ [118], greatly restricting the viable parameter space for this extreme scenario.

ACKNOWLEDGMENTS

We thank Profs. Anna Watts and Charalampos Moustakidis for valuable discussions regarding neutron star physics, and Drs. Rodrigo Vicente and Violetta Sagun for feedback. We gratefully acknowledge the support of the Dutch Research Council (NWO) through an Open Competition Domain Science-M grant, project number OCENW.M.21.375.

Appendix A: Geodesic motion around neutron stars

We consider a static, spherically symmetric and spinless NS in hydrostatic equilibrium. Under these assumptions, the stellar structure is obtained by solving the Tolman–Oppenheimer–Volkoff equations [53],

$$\begin{aligned} \frac{dP}{dr} &= -\frac{Gm_r}{r^2 c^2} (\epsilon + P) \left(1 + \frac{4\pi r^3 P}{m_r c^2}\right) \left(1 - \frac{2Gm_r}{c^2 r}\right)^{-1}, \\ \frac{dm_r}{dr} &= 4\pi r^2 \frac{\epsilon}{c^2}, \end{aligned} \quad (\text{A1})$$

where $P(r)$, $m_r(r)$, $\epsilon(r) = \rho(r)c^2$ are the pressure, enclosed mass and energy density at radius r respectively. The system is then solved given an EOS [62] $P(\epsilon)$ and by setting the core pressure/density. The latter is iteratively modified until a stable NS [129] with the target total mass is produced.

Within the neutron star, the space-time is described by the metric [53],

$$ds^2 = -\tilde{g}_{tt}(r) c^2 dt^2 + \left(1 - \frac{2Gm_r}{rc^2}\right)^{-1} dr^2 + r^2 d\Omega^2, \quad (\text{A2})$$

where the term $\tilde{g}_{tt}(r)$ is determined from the expression

$$\frac{d \ln \tilde{g}_{tt}}{dr} = -\frac{2}{\epsilon + P} \frac{dP}{dr}, \quad (\text{A3})$$

and the boundary condition $\tilde{g}_{tt}(R) = 1 - 2Gm/(c^2 R)$. Outside the star, the space-time is taken to be Schwarzschild.

The orbits of massive particles are described by the Lagrangian $\mathcal{L} = -g_{\mu\nu} \dot{x}^\mu \dot{x}^\nu$, where $g_{\mu\nu}$ are the metric contributions to the differentials $dx^\mu dx^\nu$. Standard Lagrangian analysis yields the corresponding geodesic equations of motion,

$$\left(\frac{dr}{d\tau}\right)^2 = \frac{1}{r^2} \left(1 - \frac{2Gm_r}{rc^2}\right) \left(\frac{\mathcal{E}^2 r^2}{\tilde{g}_{tt} c^2} - h_z^2 - c^2 r^2\right), \quad (\text{A4})$$

$$\left(\frac{dr}{d\phi}\right)^2 = r^2 \left(1 - \frac{2Gm_r}{rc^2}\right) \left(\frac{\mathcal{E}^2 r^2}{h_z^2 \tilde{g}_{tt} c^2} - \frac{c^2 r^2}{h_z^2} - 1\right), \quad (\text{A5})$$

where the constants \mathcal{E} , h_z represent the specific energy and angular momentum, which are obtained by exploiting time-translation and axial symmetry of Eq. (A2).

For an incoming particle in the NS frame with impact parameter b and velocity u at infinity, the constants of motion are: $\mathcal{E} = \gamma c^2$, $h_z = \gamma b u$. Then, the angle χ , drawn by an incoming particle until it reaches its closest approach r_0 , is computed by integrating Eq. (A5),

$$\chi = h_z \int_{r_0}^{\infty} \frac{(1 - 2Gm_r/(rc^2))^{-1/2}}{r \sqrt{\mathcal{E}^2 r^2 / (\tilde{g}_{tt} c^2) - c^2 r^2 - h_z^2}} dr, \quad (\text{A6})$$

where r_0 is obtained at the root of $dr/d\tau$.

Appendix B: Calculating dynamical friction

If the point of closest approach is larger than the stellar radius R , particles follow geodesics entirely defined from the equivalent Schwarzschild spacetime as for a BH with the same mass. As such, we calculate the scattering cross-section only for those orbits that can probe the NS interior. The difference is given by,

$$\delta\sigma \equiv 4\pi \left[\int_0^{b_{\text{th}}} b \cos^2 \chi_{\text{NS}} db - \int_{b_{\text{cr}}}^{b_{\text{th}}} b \cos^2 \chi_{\text{BH}} db \right], \quad (\text{B1})$$

where b_{cr} is the critical impact parameter that separates accretion from deflection on BH geometry [53], b_{th} is a threshold impact parameter below for which particles can penetrate the NS, and $\chi_{\text{NS/BH}}$ are, respectively, the angles drawn by a particle in NS or BH spacetime. Using $\delta\sigma$ on Eq. (2), we define

$$\mathbf{F}_{\text{NS}} = \mathbf{F}_{\text{BH}} + \delta\mathbf{F}, \quad (\text{B2})$$

where F_{BH} is the dynamical friction experienced by a BH. In this work, we use the fit given by Traykova *et al.* [54] for relativistic dynamical friction on BHs.

We calculate $\delta\sigma$ by substituting Eq. (A6) for the NS and BH spacetimes within Eq. (B1) and integrating in impact parameter. For the BH spacetime, we substitute $m_r(r) = m$ and $\tilde{g}_{tt} = 1 - 2Gm/(rc^2)$. For less compact stars, the impact parameter b_{th} in the integration limit is determined by requiring the turning point of the orbit to coincide with the stellar radius. This condition is obtained by setting $dr/d\tau = 0$ at $r = R$ in the Schwarzschild metric, yielding

$$b_R^2 = R^2 \left(1 + \frac{2Gm}{Rc^2 \gamma^2 \beta^2}\right) \left(1 - \frac{2Gm}{Rc^2}\right)^{-1}. \quad (\text{B3})$$

This reduces to the well-known Newtonian relation [130] in the non-relativistic limit $c \rightarrow \infty$. Note, however, that substituting b_{cr} into Eq. (A4), it becomes apparent that around a BH, the distance of closest approach for massive particles cannot be smaller than

$$r_0^{\text{min}}(\beta) = \frac{Gm}{c^2} \frac{3\gamma^2 - 4 + 3\gamma\sqrt{\gamma^2 - 8/9}}{2(\gamma^2 - 1)}. \quad (\text{B4})$$

This also suggests that particles of velocity β cannot graze the surface of a very compact NS and escape. In

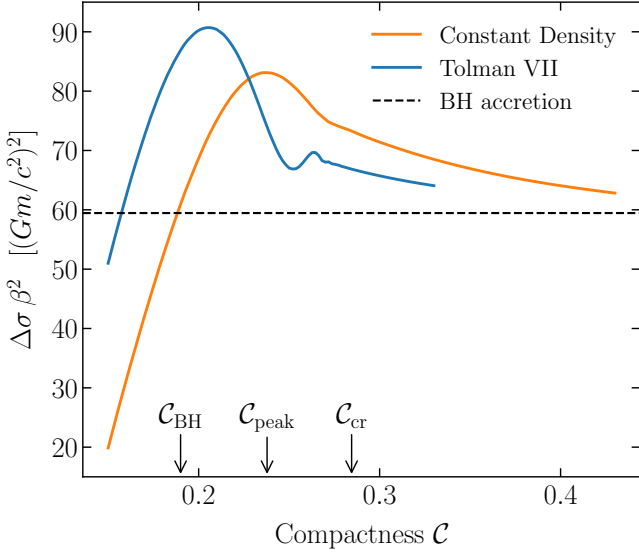


FIG. 5. **Difference in scattering cross-section for an extended toy object and a point mass.** The dashed black line represents the accretion cross-section for a BH.

particular, since $\lim_{\beta \rightarrow 0} r_0^{\min} = 4Gm/c^2$, only NSs with compactness $\mathcal{C} \geq 0.25$ can be affected.² For these stars, radial particles with $b < b_{\text{cr}}$ can still penetrate the interior, but the distance of closest approach undergoes a discontinuous jump, from $r_0^{\min}(\beta)$ to a point deep within the star when Eq. (A4) bifurcates. Physically, these particles are effectively on plunging trajectories and approach deep within the core but eventually escape due to the decrease in enclosed mass. In practice, this means that

$$b_{\text{th}}(\beta, m, R) = \begin{cases} b_R(\beta, m, R) & R \geq r_0^{\min}(\beta, m), \\ b_{\text{cr}}(\beta, m) & \text{otherwise,} \end{cases} \quad (\text{B6})$$

as long as $b_{\text{th}} < b_{\text{max}}$.

Appendix C: The compactness dependence

In this section, we provide an analytical argument to understand the observed relation between dynamical friction and NS mass seen in Fig. 1. To factor out the effect of the velocity distribution we examine the cross-section at fixed velocity.

² The effect can appear at smaller compactness if the star has a thick crust, which contributes disproportionately more to its radius than to its enclosed mass. The required condition is that Eq. (A4) exhibits a local minimum and maximum within r_0^{\min} , or equivalently that

$$\frac{dP}{dr} = \frac{\rho c^2 + P}{r} \left(1 - \frac{c^4}{\mathcal{E}^2} \tilde{g}_{\text{tt}} \right), \quad (\text{B5})$$

has two distinct and positive roots.

To demonstrate the robustness of the observed trends, we reproduce our numerical results using idealized stellar models: a constant-density sphere and a Tolman–VII configuration [131]. As is evident for the geometric unit representation of these models, they depend primarily on the compactness, with the total mass only scaling the cross-section quadratically. For realistic equations of state, and in the absence of twin-star branches [132], fixing the mass effectively fixes the radius and therefore \mathcal{C} . For concreteness, we evaluate the cross-section at the average orbital velocity of the radial snapshot in Fig. 1, which provides a representative dynamical scale for the encounters. As shown in Fig. 5, the toy-models reproduce all the characteristic features of Fig. 1. Additionally, we observe that for higher values of compactness, the scattering cross section appears to asymptotically mimic BH accretion, though we only report the behavior up to each model’s stability limit.

For reference, we define \mathcal{C}_{BH} and $\mathcal{C}_{\text{peak}}$ through the constant density model for which we report the following numerical fits

$$\mathcal{C}_{\text{peak}} \approx 0.097 + 0.48\beta - 0.47\beta^2 + 0.2\beta^3, \quad (\text{C1})$$

$$\mathcal{C}_{\text{BH}} \approx 0.04 + 0.5\beta - 0.47\beta^2 + 0.2\beta^3, \quad (\text{C2})$$

that were used to mark their respective points in Fig. 1. For completeness, the critical compactness associated with plunging trajectories is given by $\mathcal{C}_{\text{cr}} = Gm/c^2/r_0^{\min}$. In general, because of NS’s crust reduces the stellar compactness, these predictions slightly overestimate the true values for realistic EOS.

Analytical understanding. Motivated by the robustness of these trends across numerical experiments and toy models, we next develop a minimal analytical description to capture their physical origin. First, the cross-section decline at low compactness is easy to interpret: as \mathcal{C} approaches 0, the object becomes infinitely dilute and its dynamical friction vanishes, and $\lim_{\mathcal{C} \rightarrow 0} \delta\sigma = -(\sigma_{\text{BH}} + \sigma_{\text{acc}})$. For the rest, it is useful to recast Eq. (B1) in terms of the deflection angle,

$$\delta\sigma \approx \sigma_{\text{acc}} - \pi \int_0^{b_{\text{cr}}} \cos \theta_{\text{NS}} db^2, \quad (\text{C3})$$

where we have neglected a third term integrated in $b \in (b_{\text{cr}}, b_{\text{th}})$ which is either small or zero. Evidently, the signature of the remaining integral in Eq. (C3) directly determines the force hierarchy between a NS and a BH. In practice, if most of the radially infalling particles that would be accreted by a BH are instead strongly deflected by the NS on obtuse angles, the NS cross-section becomes larger. This is possible with increasing stellar compactness where deflection grows stronger, as particles probe increasingly extreme curvature just outside the NS. It also follows that, beyond a certain compactness, $\mathcal{C}_{\text{peak}}$, particles begin to wind around the star, reducing the net deflection and thereby diminishing the dynamical friction, leading to the observed peak. Finally, for extremely

compact objects, particles with $b \lesssim b_{\text{cr}}$ become effectively trapped, winding around the star for many cycles. Then, the corresponding integral averages out through rapid oscillations, leading to $\delta\sigma \approx \sigma_{\text{acc}}$ as the compactness increases.

Appendix D: The Bayesian framework

To assess the prospects of measuring the equation of state of a NS companion in an EMRI we follow the Bayesian approach described by Coogan *et al.* [32]. We assume the strain time-series measured by the detector $d(t)$ to be the sum of the signal $s(t)$ and the detector’s noise $n(t)$ which we take to be Gaussian to write the likelihood function

$$p(d|h_{\theta}) \propto \exp \left[\langle h_{\theta}|d \rangle - \langle h_{\theta}|h_{\theta} \rangle \right]. \quad (\text{D1})$$

Then, the terms $\langle a|b \rangle$ are the overlaps of two waveforms a and b in the frequency domain defined as

$$\langle a|b \rangle \equiv 4 \text{Re} \int_{f_{\min}}^{\infty} \frac{a^*(f) b(f)}{S_n(f)} df, \quad (\text{D2})$$

with $S_n(f)$ taken to be the one-sided LISA power-spectral density taken to be the Michelson-like PSD from [142], and³

$$\theta = \{M, m, \rho, d_L, \phi_c, t_c\}$$

are the parameters describing the model waveform. The binary masses M, m and a factor describing the spike’s density normalization ρ are intrinsic parameters for which the likelihood is maximized over numerically. Conversely, the binary’s luminosity distance d_L , and the waveform’s phase and time offsets ϕ_c, t_c can all be maximized analytically, to yield the new likelihood,

$$p_{\max}(d|h_{\theta}) \equiv \exp \left[\frac{\langle h_{\theta}|d \rangle_{\max}^2}{2 \langle h_{\theta}|h_{\theta} \rangle} \right], \quad (\text{D3})$$

where with the subscript “max” we indicate maximization over phase and time offsets of the signal as described in [32]. Finally, the EMRI waveforms h_{θ}, s are obtained by incorporating the angular momentum rate from Eq. (1) for each EOS into the `FastEMRIWaveforms.v2.0.0` (FEW) framework [85–88] framework, and initializing binaries 4 years before merger. Because we will be working with large SNR $\sim \sqrt{\langle d|d \rangle}$, we take $d(t) \approx s(t)$.

The posterior distribution $p(\theta|d) \propto p_{\max}(d|h_{\theta}) p(\theta)$ is explored using nested sampling [143–145] implemented

with `dynesty.v2.1.5` [146, 147]. Mapping out these posteriors allows us to assess how well the model’s parameters can be measured and whether bias is induced by performing inference with the wrong model.

The prior distributions $p(\theta)$ are taken to be uniform \mathcal{U} accordingly: $\rho = \rho_0 \mathcal{U}(8, 12)$, $M = M_0 + \mathcal{U}(-15, 15) M_{\odot}$, $m = m_0 + 10^{-5} \mathcal{U}(-11, 11) M_{\odot}$, where ρ_0, M_0, m_0 are the values of the injected parameters. These are relatively narrow to mitigate the computational cost of EMRI inference [148, 149] and isolate the effect of the internal structure.

Finally, to assess the ability to distinguish between different companion models we compute the evidence for each model/hypothesis

$$p(d) = \int p_{\max}(d|h_{\theta}) p(\theta) d\theta, \quad (\text{D4})$$

and compare them in competing pairs H_k using the Bayes factor [103], defined as the ratio

$$\mathcal{B} \equiv \frac{p(d|H_1)}{p(d|H_2)}. \quad (\text{D5})$$

A large Bayes factor denotes a confident Bayesian preference for model H_1 over H_2 .

Alternatively, a useful approximation for estimating the Bayes factor, is the Laplace approximation $\ln \mathcal{B} = \text{SNR}^2 (1 - \mathcal{F}^2)/2$ [150, 151] where \mathcal{F} is the *fitting factor* calculated by maximizing Eq. (D2) over θ and normalizing it such that $\mathcal{F} = 1$ for the same waveform.

Appendix E: Is a phenomenological measurement of the radius viable?

We now consider whether it is possible to measure properties of the NS structure, with minimal model assumptions. This approach allows constraints on the EOS without fixing it a priori. To this end, we approximate the space-time within the NS as that sourced by a generalized super-ellipsoid (“Gensel”) density profile of the form,

$$\rho(r) = \rho_c \left(1 - \frac{r^2}{R^2} \right)^a. \quad (\text{E1})$$

This family of profiles generalizes the well-known, fully analytic Tolman VII solution [131], which has been shown to approximate numerical solutions for a wide range of EOS models [59, 152]. Within this framework, the parameter a regulates the steepness with which the density tapers off towards the stellar radius, thus effectively controlling the relative size between NS core and crust: larger values of a produce thicker crusts. For $a = 0$, the model reduces to a constant density profile sourcing the interior Schwarzschild metric, and for $a = 1$, it reduces to the Tolman VII solution [153].

³ We note that changes in the slope of the cusp are mostly degenerate with the density normalization and preliminary analysis shows that they don’t affect the shape of the losses within the regions we are interested in.

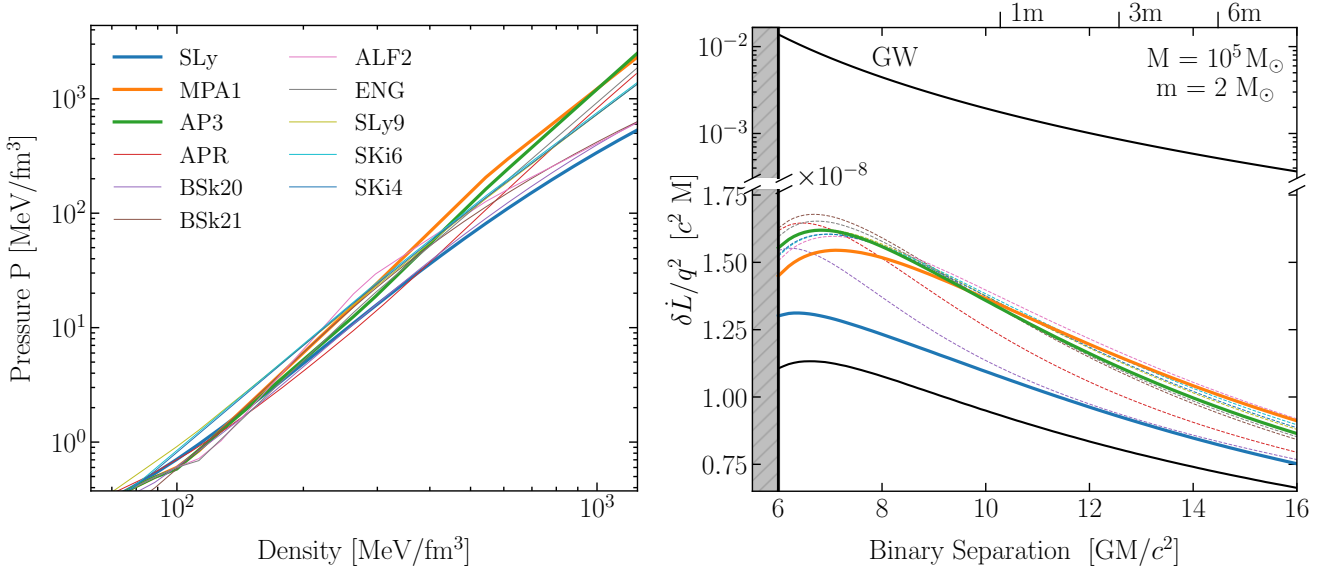


FIG. 6. **Equations of state (left) and angular-momentum loss of neutron stars as a function of binary separation (right).** For comparison, we show the corresponding accretion-driven loss for a BH of the same mass (black), as well as the loss from gravitational-wave emission, which is plotted on a disconnected y-axis on top. Along the top axis we indicate the initial separations at which a binary would plunge after the corresponding number of months. All results assume the benchmark dark-matter spike for a system with a $M = 10^5 M_\odot$ primary, representative of the density inferred for Draco dSph [104]. Aside from the three fiducial equations of state, we also show a collection of 8 other representative models: (AP4 [96], BSk20-21 [133], ALF2 [134], ENG [135], SLy9 [136], SKi6 [137], SKi4 [138]) using unified [133, 139, 140] and polytrope [136, 141] modelling with a crust as in [98].

We find the mass enclosed within radius r to be given analytically by,

$$m_r(r) = \frac{4\pi\rho_c r^3}{3} {}_2F_1\left(-a, 3/2, 5/2, r^2/R^2\right), \quad (\text{E2})$$

where it is useful to eliminate the central density ρ_c from the expressions by substituting it with the total mass,

$$M = \frac{4\pi\rho_c R^3}{3} \frac{\Gamma(5/2)\Gamma(a+1)}{\Gamma(a+5/2)}. \quad (\text{E3})$$

It is straightforward to obtain a closed form expression for g_{rr} by substituting Eq. (E2) into Eq. (A2), but we must integrate Eq. (A3) numerically for g_{tt} after computing $P(r)$ imposing $P(R) = 0$.⁴ We then proceed to solve the geodesic motion of particles within our modified model to compute dynamical friction and produce relativistic waveforms for inspirals within DM spikes.

In Fig. 7, we show the two-dimensional marginal posteriors of the NS radius, and DM density where we have marginalized over the gensel slope parameter. The posteriors are obtained by injecting the three fiducial NS systems and recovering them with our modified model. For simplicity, and given the small inferred bias in primary

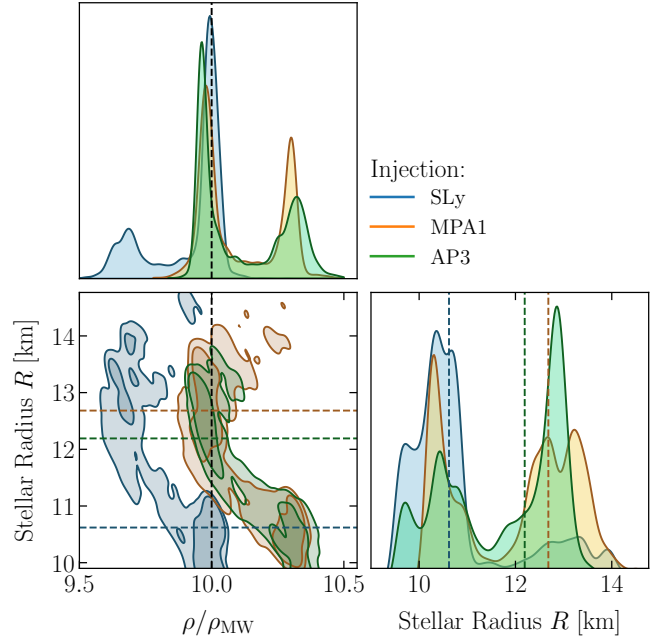


FIG. 7. **Marginal posteriors for neutron star radius and the spike's density.** Dashed lines indicate true values.

⁴ We omit closed-form expressions for $P(r)$ and $g_{tt}(r)$ as they are algebraically unwieldy.

and secondary mass (cf. Fig. 2), we fix these two parameters in this calculation to their true value ($M = 10^6 M_\odot$ and $m = 2 M_\odot$). Evidently, while there can be cases (SLy) where the posteriors are very informative about the stellar radius, encompassing it within roughly a 500 m uncertainty, in the other two cases we have tested they are not informative. In both the MPA1 and AP3 we ob-

serve the gensel model to be very degenerate between the DM density and the stellar radius, producing strong bimodality. Such degeneracy is however absent when testing specific EOS against each other where the radius of the NS is fixed for a given mass. In light of these results, we consider a target-based comparison more appropriate than a phenomenological one.

-
- [1] Monica Colpi *et al.* (LISA), “LISA Definition Study Report,” (2024), [arXiv:2402.07571 \[astro-ph.CO\]](#).
 - [2] Jun Luo *et al.* (TianQin), “TianQin: a space-borne gravitational wave detector,” *Class. Quant. Grav.* **33**, 035010 (2016), [arXiv:1512.02076 \[astro-ph.IM\]](#).
 - [3] Wen-Rui Hu and Yue-Liang Wu, “The Taiji Program in Space for gravitational wave physics and the nature of gravity,” *Natl. Sci. Rev.* **4**, 685–686 (2017).
 - [4] Vitor Cardoso and Andrea Maselli, “Constraints on the astrophysical environment of binaries with gravitational wave observations,” *Astron. Astrophys.* **644**, A147 (2020), [arXiv:1909.05870 \[astro-ph.HE\]](#).
 - [5] K. G. Arun *et al.* (LISA), “New horizons for fundamental physics with LISA,” *Living Rev. Rel.* **25**, 4 (2022), [arXiv:2205.01597 \[gr-qc\]](#).
 - [6] Giada Caneva Santoro, Soumen Roy, Rodrigo Vicente, Maria Haney, Ornella Juliana Piccinni, Walter Del Pozzo, and Mario Martinez, “First Constraints on Compact Binary Environments from LIGO-Virgo Data,” *Phys. Rev. Lett.* **132**, 251401 (2024), [arXiv:2309.05061 \[gr-qc\]](#).
 - [7] Gianfranco Bertone, “Dark matter, black holes, and gravitational waves,” *Nucl. Phys. B* **1003**, 116487 (2024), [arXiv:2404.11513 \[astro-ph.CO\]](#).
 - [8] Lorenz Zwick, János Takátsy, Pankaj Saini, Kai Hendriks, Johan Samsing, Christopher Tiede, Connor Rowan, and Alessandro A. Trani, “Environmental effects in stellar mass gravitational wave sources I: Expected fraction of signals with significant dephasing in the dynamical and AGN channels,” (2025), [arXiv:2503.24084 \[astro-ph.HE\]](#).
 - [9] Vitor Cardoso, Kyriakos Destounis, Francisco Duque, Rodrigo Panosso Macedo, and Andrea Maselli, “Black holes in galaxies: Environmental impact on gravitational-wave generation and propagation,” *Physical Review D* **105** (2022), [10.1103/physrevd.105.1061501](#).
 - [10] Thomas F. M. Spieksma, Vitor Cardoso, Gregorio Carullo, Matteo Della Rocca, and Francisco Duque, “Black hole spectroscopy in environments: detectability prospects,” (2025), [arXiv:2409.05950 \[gr-qc\]](#).
 - [11] Philippa S. Cole, Gianfranco Bertone, Adam Coogan, Daniele Gaggero, Theophanes Karydas, Bradley J. Kavanagh, Thomas F. M. Spieksma, and Giovanni Maria Tomaselli, “Distinguishing environmental effects on binary black hole gravitational waveforms,” *Nature Astron.* **7**, 943–950 (2023), [arXiv:2211.01362 \[gr-qc\]](#).
 - [12] Soumen Roy and Rodrigo Vicente, “Compact binary coalescences in dense gaseous environments can pose as ones in vacuum,” *Phys. Rev. D* **111**, 084037 (2025), [arXiv:2410.16388 \[gr-qc\]](#).
 - [13] Pau Amaro-Seoane, Jonathan R. Gair, Marc Freitag, M Coleman Miller, Ilya Mandel, Curt J Cutler, and Stanislav Babak, “Intermediate and extreme mass-ratio inspirals—astrophysics, science applications and detection using lisa,” *Classical and Quantum Gravity* **24**, R113–R169 (2007).
 - [14] Jonathan R. Gair, Michele Vallisneri, Shane L. Larson, and John G. Baker, “Testing general relativity with low-frequency, space-based gravitational-wave detectors,” *Living Reviews in Relativity* **16** (2013), [10.12942/lrr-2013-7](#).
 - [15] Lorenzo Speri, Susanna Barsanti, Andrea Maselli, Thomas P. Sotiriou, Niels Warburton, Maarten van de Meent, Alvin J. K. Chua, Ollie Burke, and Jonathan Gair, “Probing fundamental physics with extreme mass ratio inspirals: a full bayesian inference for scalar charge,” (2024), [arXiv:2406.07607 \[gr-qc\]](#).
 - [16] Soumodeep Mitra, Sumanta Chakraborty, Rodrigo Vicente, and Justin C. Feng, “Probing the quantum nature of black holes with ultralight boson environments,” *Physical Review D* **110** (2024), [10.1103/physrevd.110.084012](#).
 - [17] Francisco Duque, Caio F. B. Macedo, Rodrigo Vicente, and Vitor Cardoso, “Extreme-mass-ratio inspirals in ultralight dark matter,” *Phys. Rev. Lett.* **133**, 121404 (2024).
 - [18] Leor et al. Barack, “Black holes, gravitational waves and fundamental physics: a roadmap,” *Classical and Quantum Gravity* **36**, 143001 (2019).
 - [19] Gianfranco Bertone, Djuna Croon, Mustafa Amin, Kimberly K. Boddy, Bradley Kavanagh, Katherine J. Mack, Priyamvada Natarajan, Toby Opferkuch, Katelin Schutz, Volodymyr Takhistov, Christoph Weniger, and Tien-Tien Yu, “Gravitational wave probes of dark matter: challenges and opportunities,” *SciPost Physics Core* **3** (2020), [10.21468/scipostphyscore.3.2.007](#).
 - [20] Daniel Baumann, Gianfranco Bertone, John Stout, and Giovanni Maria Tomaselli, “Ionization of gravitational atoms,” *Physical Review D* **105** (2022), [10.1103/physrevd.105.115036](#).
 - [21] Andrea Maselli, Nicola Franchini, Leonardo Gualtieri, Thomas P. Sotiriou, Susanna Barsanti, and Paolo Pani, “Detecting fundamental fields with lisa observations of gravitational waves from extreme mass-ratio inspirals,” *Nature Astronomy* **6**, 464–470 (2022).
 - [22] Andrew L. Miller, “Gravitational wave probes of particle dark matter: a review,” (2025), [arXiv:2503.02607 \[astro-ph.HE\]](#).
 - [23] Paolo Gondolo and Joseph Silk, “Dark matter annihilation at the galactic center,” *Physical Review Letters* **83**, 1719–1722 (1999).
 - [24] HongSheng Zhao and Joseph Silk, “Dark minihalos with intermediate mass black holes,” *Physical Review Letters*

- 95** (2005), 10.1103/physrevlett.95.011301.
- [25] Gianfranco Bertone, Andrew R. Zentner, and Joseph Silk, “A new signature of dark matter annihilations: gamma-rays from intermediate-mass black holes,” *Phys. Rev. D* **72**, 103517 (2005), arXiv:astro-ph/0509565.
 - [26] Laleh Sadeghian, Francesc Ferrer, and Clifford M. Will, “Dark-matter distributions around massive black holes: A general relativistic analysis,” *Physical Review D* **88** (2013), 10.1103/physrevd.88.063522.
 - [27] Francesc Ferrer, Augusto Medeiros da Rosa, and Clifford M. Will, “Dark matter spikes in the vicinity of kerr black holes,” *Physical Review D* **96** (2017), 10.1103/physrevd.96.083014.
 - [28] Gianfranco Bertone, A. Renske A. C. Wierda, Daniele Gaggero, Bradley J. Kavanagh, Marta Volonteri, and Naoki Yoshida, “Dark matter mounds: towards a realistic description of dark matter overdensities around black holes,” (2024), arXiv:2404.08731 [astro-ph.CO].
 - [29] Piero Ullio, HongSheng Zhao, and Marc Kamionkowski, “Dark-matter spike at the galactic center?” *Physical Review D* **64** (2001), 10.1103/physrevd.64.043504.
 - [30] Kazunari Eda, Yousuke Itoh, Sachiko Kuroyanagi, and Joseph Silk, “New Probe of Dark-Matter Properties: Gravitational Waves from an Intermediate-Mass Black Hole Embedded in a Dark-Matter Minispike,” *Phys. Rev. Lett.* **110**, 221101 (2013), arXiv:1301.5971 [gr-qc].
 - [31] Bradley J. Kavanagh, David A. Nichols, Gianfranco Bertone, and Daniele Gaggero, “Detecting dark matter around black holes with gravitational waves: Effects of dark-matter dynamics on the gravitational waveform,” *Physical Review D* **102** (2020), 10.1103/physrevd.102.083006.
 - [32] Adam Coogan, Gianfranco Bertone, Daniele Gaggero, Bradley J. Kavanagh, and David A. Nichols, “Measuring the dark matter environments of black hole binaries with gravitational waves,” *Physical Review D* **105** (2022), 10.1103/physrevd.105.043009.
 - [33] Philippa S. Cole, Adam Coogan, Bradley J. Kavanagh, and Gianfranco Bertone, “Measuring dark matter spikes around primordial black holes with einstein telescope and cosmic explorer,” *Physical Review D* **107** (2023), 10.1103/physrevd.107.083006.
 - [34] Theophanes K. Karydas, Bradley J. Kavanagh, and Gianfranco Bertone, “Sharpening the dark matter signature in gravitational waveforms. I. Accretion and eccentricity evolution,” (2025), arXiv:2402.13053 [gr-qc].
 - [35] Bradley J. Kavanagh, Theophanes K. Karydas, Gianfranco Bertone, Pierfrancesco Di Cintio, and Mario Pasquato, “Sharpening the dark matter signature in gravitational waveforms ii: Numerical simulations with the nbodimri code,” (2024), arXiv:2402.13762 [gr-qc].
 - [36] Nicholas Speeney, Andrea Antonelli, Vishal Baibhav, and Emanuele Berti, “Impact of relativistic corrections on the detectability of dark-matter spikes with gravitational waves,” *Physical Review D* **106** (2022), 10.1103/physrevd.106.044027.
 - [37] Niklas Becker, Laura Sagunski, Lukas Prinz, and Saeed Rastgoo, “Circularization versus eccentricification in intermediate mass ratio inspirals inside dark matter spikes,” *Physical Review D* **105** (2022), 10.1103/physrevd.105.063029.
 - [38] Soumodeep Mitra, Nicholas Speeney, Sumanta Chakraborty, and Emanuele Berti, “Extreme mass ratio inspirals in rotating dark matter spikes,” (2025), arXiv:2505.04697 [gr-qc].
 - [39] Gen-Liang Li, Yong Tang, and Yue-Liang Wu, “Probing dark matter spikes via gravitational waves of extreme-mass-ratio inspirals,” *Science China Physics, Mechanics & Astronomy* **65** (2022), 10.1007/s11433-022-1930-9.
 - [40] Zi-Chang Zhang and Yong Tang, “Velocity distribution of dark matter in spikes around schwarzschild black holes and effects on gravitational waves from extreme-mass-ratio inspirals,” *Physical Review D* **110** (2024), 10.1103/physrevd.110.103008.
 - [41] Diptajyoti Mukherjee, A Miguel Holgado, Go Ogiya, and Hy Trac, “Examining the effects of dark matter spikes on eccentric intermediate-mass ratio inspirals using n-body simulations,” *Monthly Notices of the Royal Astronomical Society* **533**, 2335–2355 (2024).
 - [42] Otto A. Hannuksela, Kenny C. Y. Ng, and Tjonnie G. F. Li, “Extreme dark matter tests with extreme mass ratio inspirals,” *Physical Review D* **102** (2020), 10.1103/physrevd.102.103022.
 - [43] Niklas Becker and Laura Sagunski, “Comparing accretion disks and dark matter spikes in intermediate mass ratio inspirals,” *Physical Review D* **107** (2023), 10.1103/physrevd.107.083003.
 - [44] Yu-Chen Zhou, Hong-Bo Jin, Cong-Feng Qiao, and Yue-Liang Wu, “Intermediate-mass-ratio inspirals with general dynamical friction in dark matter minispikes,” (2025), arXiv:2405.19240 [astro-ph.HE].
 - [45] David A. Nichols, Benjamin A. Wade, and Alexander M. Grant, “Secondary accretion of dark matter in intermediate mass-ratio inspirals: Dark-matter dynamics and gravitational-wave phase,” *Physical Review D* **108** (2023), 10.1103/physrevd.108.124062.
 - [46] Thomas D. P. Edwards, Marco Chianese, Bradley J. Kavanagh, Samaya M. Nissanke, and Christoph Weniger, “Unique multimessenger signal of qcd axion dark matter,” *Physical Review Letters* **124** (2020), 10.1103/physrevlett.124.161101.
 - [47] Diego Montalvo, Adam Smith-Orlik, Saeed Rastgoo, Laura Sagunski, Niklas Becker, and Hazkeel Khan, “Post-newtonian effects in compact binaries with a dark matter spike: A lagrangian approach,” *Universe* **10**, 427 (2024).
 - [48] Rodrigo Vicente, Theophanes K. Karydas, and Gianfranco Bertone, “Fully relativistic treatment of extreme mass-ratio inspirals in collisionless environments,” *Phys. Rev. Lett.* **135**, 211401 (2025).
 - [49] Theophanes K. Karydas, Rodrigo Vicente, and Gianfranco Bertone, “Mass and spin coevolution of black holes inspiralling through dark matter,” (2025), arXiv:2510.13604 [gr-qc].
 - [50] S. Chandrasekhar, “Dynamical Friction. I. General Considerations: the Coefficient of Dynamical Friction.” *apj* **97**, 255 (1943).
 - [51] S. Chandrasekhar, “Dynamical Friction. II. The Rate of Escape of Stars from Clusters and the Evidence for the Operation of Dynamical Friction.” *Astrophys. J.* **97**, 263 (1943).
 - [52] S. Chandrasekhar, “Dynamical Friction. III. a More Exact Theory of the Rate of Escape of Stars from Clusters.” *Astrophys. J.* **98**, 54 (1943).
 - [53] Charles W. Misner, K. S. Thorne, and J. A. Wheeler, *Gravitation* (W. H. Freeman, San Francisco, 1973).
 - [54] Dina Traykova, Rodrigo Vicente, Katy Clough, Thomas Helfer, Emanuele Berti, Pedro G. Ferreira, and Lam

- Hui, “Relativistic drag forces on black holes from scalar dark matter clouds of all sizes,” *Physical Review D* **108** (2023), 10.1103/physrevd.108.1121502.
- [55] Conor Dyson, Jaime Redondo-Yuste, Maarten van de Meent, and Vitor Cardoso, “Relativistic aerodynamics of spinning black holes,” *Phys. Rev. D* **109**, 104038 (2024), arXiv:2402.07981 [gr-qc].
- [56] L. Filipe O. Costa, Rita Franco, and Vitor Cardoso, “Gravitational magnus effect,” *Physical Review D* **98** (2018), 10.1103/physrevd.98.024026.
- [57] Zipeng Wang, Thomas Helfer, Dina Traykova, Katy Clough, and Emanuele Berti, “Gravitational magnus effect from scalar dark matter,” (2024), arXiv:2402.07977 [gr-qc].
- [58] Patryk Mach, Mehrab Momennia, and Olivier Sarbach, “Accretion of a vlasov gas by a kerr black hole,” (2025), arXiv:2508.04783 [gr-qc].
- [59] J. M. Lattimer and M. Prakash, “Neutron star structure and the equation of state,” *The Astrophysical Journal* **550**, 426–442 (2001).
- [60] J. M. Lattimer and M. Prakash, “The physics of neutron stars,” *Science* **304**, 536–542 (2004).
- [61] Katerina Chatziioannou, H. Thankful Cromartie, Stefano Gandolfi, Ingo Tews, David Radice, Andrew W. Steiner, and Anna L. Watts, “Neutron stars and the dense matter equation of state: from microscopic theory to macroscopic observations,” (2024), arXiv:2407.11153 [nucl-th].
- [62] Feryal Özel and Paulo Freire, “Masses, radii, and the equation of state of neutron stars,” *Annual Review of Astronomy and Astrophysics* **54**, 401–440 (2016).
- [63] V. Dexheimer, R. O. Gomes, T. Klähn, S. Han, and M. Salinas, “Gw190814 as a massive rapidly rotating neutron star with exotic degrees of freedom,” *Phys. Rev. C* **103**, 025808 (2021).
- [64] Eemeli Annala, Tyler Gorda, Aleks Kurkela, Joonas Nättilä, and Aleks Vuorinen, “Evidence for quark-matter cores in massive neutron stars,” *Nature Physics* **16**, 907–910 (2020).
- [65] Joseph Bramante and Nirmal Raj, “Dark matter in compact stars,” *Physics Reports* **1052**, 1–48 (2024), dark matter in compact stars.
- [66] Kilar Zhang, Ling-Wei Luo, Jie-Shiun Tsao, Chian-Shu Chen, and Feng-Li Lin, “Dark stars and gravitational waves: Topical review,” *Results in Physics* **53**, 106967 (2023).
- [67] V. Dexheimer, L. T. T. Soethe, J. Roark, R. O. Gomes, S. O. Kepler, and S. Schramm, “Phase transitions in neutron stars,” *International Journal of Modern Physics E* **27**, 1830008 (2018).
- [68] R. Alves Batista, M. A. Amin, G. Barenboim, N. Bartolo, and et al., “Euclpt white paper: Opportunities and challenges for theoretical astroparticle physics in the next decade,” (2021), arXiv:2110.10074 [astro-ph.HE].
- [69] Geert Raaijmakers, Samaya Nissanke, Francois Foucart, Mansi M. Kasliwal, Mattia Bulla, Rodrigo Fernández, Amelia Henkel, Tanja Hinderer, Kenta Hotokezaka, Kamilė Lukošiušė, Tejaswi Venumadhav, Sarah Antier, Michael W. Coughlin, Tim Dietrich, and Thomas D. P. Edwards, “The challenges ahead for multimessenger analyses of gravitational waves and kilonova: A case study on gw190425,” *The Astrophysical Journal* **922**, 269 (2021).
- [70] B. S. Sathyaprakash, Matthew Bailes, Mansi M. Kasliwal, Samaya Nissanke, Shreya Anand, Igor Andreoni, Monica Colpi, Michael Coughlin, Evan Hall, Vicky Kalogera, Dan Kasen, and Alberto Sesana, “Multimessenger universe with gravitational waves from binaries,” (2019), arXiv:1903.09277 [astro-ph.HE].
- [71] David Shoemaker (LIGO Scientific), “Gravitational wave astronomy with LIGO and similar detectors in the next decade,” (2019), arXiv:1904.03187 [gr-qc].
- [72] F. Acernese *et al.* (VIRGO), “Advanced Virgo: a second-generation interferometric gravitational wave detector,” *Class. Quant. Grav.* **32**, 024001 (2015), arXiv:1408.3978 [gr-qc].
- [73] T. Akutsu *et al.* (KAGRA), “Overview of KAGRA : KAGRA science,” (2020), arXiv:2008.02921 [gr-qc].
- [74] Gabriel Andres Piovano, Andrea Maselli, and Paolo Pani, “Constraining the tidal deformability of supermassive objects with extreme mass ratio inspirals and semianalytical frequency-domain waveforms,” *Phys. Rev. D* **107**, 024021 (2023).
- [75] B. P. Abbott and et al. (LIGO Scientific Collaboration and Virgo Collaboration), “Gw170817: Observation of gravitational waves from a binary neutron star inspiral,” *Phys. Rev. Lett.* **119**, 161101 (2017).
- [76] Bhaskar Biswas and Stephan Rosswog, “Simultaneously constraining the neutron star equation of state and mass distribution through multimessenger observations and nuclear benchmarks,” (2025), arXiv:2408.15192 [astro-ph.HE].
- [77] B. P. Abbott and et al., “Gw190425: Observation of a compact binary coalescence with total mass $3.4 m_{\odot}$,” *The Astrophysical Journal Letters* **892**, L3 (2020).
- [78] B. P. Abbott, R. Abbott, T. D. Abbott, F. Acernese, K. Ackley, C. Adams, and Adams, “Gw170817: Measurements of neutron star radii and equation of state,” *Physical Review Letters* **121** (2018), 10.1103/physrevlett.121.161101.
- [79] David Radice, Albino Perego, Francesco Zappa, and Sebastiano Bernuzzi, “Gw170817: Joint constraint on the neutron star equation of state from multimessenger observations,” *The Astrophysical Journal Letters* **852**, L29 (2018).
- [80] G. Raaijmakers, S. K. Greif, T. E. Riley, T. Hinderer, K. Hebeler, A. Schwenk, A. L. Watts, S. Nissanke, S. Guillot, J. M. Lattimer, and R. M. Ludlam, “Constraining the dense matter equation of state with joint analysis of nicer and ligo/virgo measurements,” *The Astrophysical Journal Letters* **893**, L21 (2020).
- [81] Paolo Pani and Andrea Maselli, “Love in extrema ratio,” *International Journal of Modern Physics D* **28**, 1944001 (2019).
- [82] Hassan Khalvati, Alessandro Santini, Francisco Duque, Lorenzo Speri, Jonathan Gair, Huan Yang, and Richard Brito, “Impact of relativistic waveforms in lisa’s science objectives with extreme-mass-ratio inspirals,” *Physical Review D* **111** (2025), 10.1103/physrevd.111.082010.
- [83] Scott A. Hughes, Steve Drasco, Éanna É. Flanagan, and Joel Franklin, “Gravitational radiation reaction and inspiral waveforms in the adiabatic limit,” *Physical Review Letters* **94** (2005), 10.1103/physrevlett.94.221101.
- [84] Brandon Carter, “Global structure of the kerr family of gravitational fields,” *Phys. Rev.* **174**, 1559–1571 (1968).

- [85] Michael L. Katz, Alvin J. K. Chua, Lorenzo Speri, Niels Warburton, and Scott A. Hughes, “Fast extreme-mass-ratio-inspiral waveforms: New tools for millihertz gravitational-wave data analysis,” *Phys. Rev. D* **104**, 064047 (2021), [arXiv:2104.04582 \[gr-qc\]](#).
- [86] Alvin J. K. Chua, Michael L. Katz, Niels Warburton, and Scott A. Hughes, “Rapid generation of fully relativistic extreme-mass-ratio-inspiral waveform templates for lisa data analysis,” *Physical Review Letters* **126** (2021), [10.1103/physrevlett.126.051102](#).
- [87] Lorenzo Speri, Michael L. Katz, Alvin J. K. Chua, Scott A. Hughes, Niels Warburton, Jonathan E. Thompson, Christian E. A. Chapman-Bird, and Jonathan R. Gair, “Fast and fourier: extreme mass ratio inspiral waveforms in the frequency domain,” *Frontiers in Applied Mathematics and Statistics* **9** (2024), [10.3389/fams.2023.1266739](#).
- [88] Christian E. A. Chapman-Bird, Lorenzo Speri, Zachary Nasipak, Ollie Burke, Michael L. Katz, Alessandro Santini, Shubham Kejriwal, Philip Lynch, Josh Mathews, Hassan Khalvati, Jonathan E. Thompson, Soichiro Isoyama, Scott A. Hughes, Niels Warburton, Alvin J. K. Chua, and Maxime Pigou, “The fast and the frame-dragging: Efficient waveforms for asymmetric-mass eccentric equatorial inspirals into rapidly-spinning black holes,” (2025), [arXiv:2506.09470 \[gr-qc\]](#).
- [89] W. A. Mulder, “Dynamical friction on extended objects,” *AAP* **117**, 9–16 (1983).
- [90] B Morton, S Khochfar, and J Oñorbe, “Gaseous dynamical friction: a numerical study of extended perturbers,” *Monthly Notices of the Royal Astronomical Society* **541**, 396–408 (2025).
- [91] V. M. Gorkavenko, A. I. Yakimenko, A. O. Zaporozhchenko, and E. V. Gorbar, “Dynamical friction in ultralight dark matter: Plummer sphere perspective,” (2025), [arXiv:2412.15428 \[astro-ph.GA\]](#).
- [92] James Binney and Scott Tremaine, *Galactic Dynamics: Second Edition* (Princeton University Press, 2008).
- [93] Bhaskar Biswas, “Bayesian Model Selection of Neutron Star Equations of State Using Multimessenger Observations,” *Astrophys. J.* **926**, 75 (2022), [arXiv:2106.02644 \[astro-ph.HE\]](#).
- [94] John Antoniadis, Paulo C. C. Freire, Norbert Wex, Thomas M. Tauris, Ryan S. Lynch, Marten H. van Kerkwijk, Michael Kramer, Cees Bassa, Vik S. Dhillon, Thomas Driebe, Jason W. T. Hessels, Victoria M. Kaspi, Vladislav I. Kondratiev, Norbert Langer, Thomas R. Marsh, Maura A. McLaughlin, Timothy T. Pennucci, Scott M. Ransom, Ingrid H. Stairs, Joeri van Leeuwen, Joris P. W. Verbiest, and David G. Whelan, “A massive pulsar in a compact relativistic binary,” *Science* **340** (2013), [10.1126/science.1233232](#).
- [95] H. M  ther, M. Prakash, and T.L. Ainsworth, “The nuclear symmetry energy in relativistic brueckner-hartree-fock calculations,” *Physics Letters B* **199**, 469–474 (1987).
- [96] A. Akmal, V. R. Pandharipande, and D. G. Ravenhall, “Equation of state of nucleon matter and neutron star structure,” *Physical Review C* **58**, 1804–1828 (1998).
- [97] P. Haensel and A. Y. Potekhin, “Analytical representations of unified equations of state of neutron-star matter,” *Astronomy & Astrophysics* **428**, 191–197 (2004).
- [98] F. Douchin and P. Haensel, “A unified equation of state of dense matter and neutron star structure,” *Astronomy & Astrophysics* **380**, 151–167 (2001).
- [99] Stanislav Babak, Jonathan Gair, Alberto Sesana, Enrico Barausse, Carlos F. Sopuerta, Christopher P. L. Berry, Emanuele Berti, Pau Amaro-Seoane, Antoine Petiteau, and Antoine Klein, “Science with the space-based interferometer lisa. v. extreme mass-ratio inspirals,” *Physical Review D* **95** (2017), [10.1103/physrevd.95.103012](#).
- [100] Davide Mancieri, Luca Broggi, Matteo Bonetti, and Alberto Sesana, “Hanging on the cliff: Extreme mass ratio inspiral formation with local two-body relaxation and post-newtonian dynamics,” *Astronomy & Astrophysics* **694**, A272 (2025).
- [101] Giovanni Mazzolari, Matteo Bonetti, Alberto Sesana, Riccardo M Colombo, Massimo Dotti, Giuseppe Lodato, and David Izquierdo-Villalba, “Extreme mass ratio inspirals triggered by massive black hole binaries: from relativistic dynamics to cosmological rates,” *Monthly Notices of the Royal Astronomical Society* **516**, 1959–1976 (2022).
- [102] Danor Aharon and Hagai B. Perets, “The impact of mass segregation and star formation on the rates of gravitational-wave sources from extreme mass ratio inspirals,” *The Astrophysical Journal Letters* **830**, L1 (2016).
- [103] Harold Jeffreys, *Theory of Probability* (Oxford University Press, Oxford, England, 1939).
- [104] Mark Wanders, Gianfranco Bertone, Marta Volonteri, and Christoph Weniger, “No wimp mini-spikes in dwarf spheroidal galaxies,” *Journal of Cosmology and Astroparticle Physics* **2015**, 004–004 (2015).
- [105] Charles Alcock, Edward Farhi, and Angela Olinto, “Strange Stars,” *Astrophys. J.* **310**, 261 (1986).
- [106] P. Haensel, J. L. Zdunik, and R. Schaefer, “Strange quark stars,” *AAP* **160**, 121–128 (1986).
- [107] Phillippe Jetzer, “Boson stars,” *Physics Reports* **220**, 163–227 (1992).
- [108] Felix Kling and Arvind Rajaraman, “Profiles of boson stars with self-interactions,” *Phys. Rev. D* **97**, 063012 (2018).
- [109] Cosimo Bambi, Ramy Brustein, Vitor Cardoso, Andrew Chael, Ulf Danielsson, Suvendu Giri, Anuradha Gupta, Pierre Heidmann, Luis Lehner, Steven Liebling, Andrea Maselli, Elisa Maggio, Samir Mathur, Lia Medeiros, Alex B. Nielsen, H  ctor R. Olivares-S  nchez, Paolo Pani, Nils Siemonsen, and George N. Wong, “Black hole mimickers: from theory to observation,” (2025), [arXiv:2505.09014 \[gr-qc\]](#).
- [110] Pawel O. Mazur and Emil Mottola, “Gravitational vacuum condensate stars,” *Proceedings of the National Academy of Sciences* **101**, 9545–9550 (2004), <https://www.pnas.org/doi/pdf/10.1073/pnas.0402717101>.
- [111] Sidney R. Coleman, “Q-balls,” *Nucl. Phys. B* **262**, 263 (1985), [Addendum: *Nucl.Phys.B* 269, 744 (1986)].
- [112] Asimina Arvanitaki, Masha Baryakhtar, and Xinlu Huang, “Discovering the qcd axion with black holes and gravitational waves,” *Physical Review D* **91** (2015), [10.1103/physrevd.91.084011](#).
- [113] Richard Brito, Vitor Cardoso, and Paolo Pani, *Superradiance: New Frontiers in Black Hole Physics* (Springer International Publishing, 2020).
- [114] Bernard Carr, Kazunori Kohri, Yuuiti Sendouda, and Jun’ichi Yokoyama, “Constraints on primordial black holes,” *Rept. Prog. Phys.* **84**, 116902 (2021),

- arXiv:2002.12778 [astro-ph.CO].
- [115] Anne M Green and Bradley J Kavanagh, “Primordial black holes as a dark matter candidate,” *Journal of Physics G: Nuclear and Particle Physics* **48**, 043001 (2021).
 - [116] I. Goldman and S. Nussinov, “Weakly Interacting Massive Particles and Neutron Stars,” *Phys. Rev. D* **40**, 3221–3230 (1989).
 - [117] Gianfranco Bertone and Malcolm Fairbairn, “Compact Stars as Dark Matter Probes,” *Phys. Rev. D* **77**, 043515 (2008), arXiv:0709.1485 [astro-ph].
 - [118] E. Aprile, K. Abe, F. Agostini, S. Ahmed Maouloud, L. Althueser, B. Andrieu, E. Angelino, J. R. Angevaere, V. C. Antochi, D. Antón Martín, F. Arneodo, L. Baudis, A. L. Baxter, M. Bazyk, L. Bellagamba, R. Biondi, A. Bismark, E. J. Brookes, A. Brown, S. Bruenner, G. Bruno, R. Budnik, T. K. Bui, C. Cai, J. M. R. Cardoso, D. Cichon, A. P. Cimental Chavez, A. P. Colijn, J. Conrad, J. J. Cuenca-García, J. P. Cussonneau, V. D’Andrea, M. P. Decowski, P. Di Gangi, S. Di Pede, S. Diglio, K. Eitel, A. Elykov, S. Farrell, A. D. Ferella, C. Ferrari, H. Fischer, M. Flierman, W. Fulgione, C. Fuselli, P. Gaemers, R. Gaior, A. Gallo Rosso, M. Galloway, F. Gao, R. Glade-Beucke, L. Grandi, J. Grigat, H. Guan, M. Guida, R. Hammann, A. Higuera, C. Hils, L. Hoetzs, N. F. Hood, J. Howlett, M. Iacovacci, Y. Itow, J. Jakob, F. Joerg, A. Joy, N. Kato, M. Kara, P. Kavargin, S. Kazama, M. Kobayashi, G. Koltman, A. Kopec, F. Kuger, H. Landsman, R. F. Lang, L. Levinson, I. Li, S. Li, S. Liang, S. Lindemann, M. Lindner, K. Liu, J. Loizeau, F. Lombardi, J. Long, J. A. M. Lopes, Y. Ma, C. Macolino, J. Mahlstedt, A. Mancosia, L. Manenti, F. Marignetti, T. Marrodán Undagoitia, K. Martens, J. Masbou, D. Masson, E. Masson, S. Mastroianni, M. Messina, K. Miuchi, K. Mizukoshi, A. Molinari, S. Moriyama, K. Morã, Y. Mosbacher, M. Murra, J. Müller, K. Ni, U. Oberlack, B. Paetsch, J. Palacio, R. Peres, C. Peters, J. Pienaar, M. Pierre, V. Pizzella, G. Plante, J. Qi, J. Qin, D. Ramírez García, R. Singh, L. Sanchez, J. M. F. dos Santos, I. Sarnoff, G. Sartorelli, J. Schreiner, D. Schulte, P. Schulte, H. Schulze Eifling, M. Schumann, L. Scotto Lavina, M. Selvi, F. Semeria, P. Shagin, S. Shi, E. Shockley, M. Silva, H. Simgen, A. Takeda, P.-L. Tan, A. Terliuk, D. Thers, F. Toschi, G. Trinchero, C. Tunnell, F. Tönnies, K. Valerius, G. Volta, C. Weinheimer, M. Weiss, D. Wenz, C. Witweg, T. Wolf, V. H. S. Wu, Y. Xing, D. Xu, Z. Xu, M. Yamashita, L. Yang, J. Ye, L. Yuan, G. Zavattini, M. Zhong, and T. Zhu, “First dark matter search with nuclear recoils from the xenonn experiment,” *Physical Review Letters* **131** (2023), 10.1103/physrevlett.131.041003.
 - [119] James B. Hartle and Kip S. Thorne, “Slowly Rotating Relativistic Stars. II. Models for Neutron Stars and Supermassive Stars,” *Astrophys. J.* **153**, 807 (1968).
 - [120] Carlos Conde-Ocazonez, Tuojin Yin, Jaquelyn Noronha-Hostler, and Nicolás Yunes, “Highly-accurate neutron star modeling in the hartle-thorne approximation,” *Phys. Rev. D* **112**, 044063 (2025).
 - [121] Norman K. Glendenning, “Limiting rotational period of neutron stars,” *Phys. Rev. D* **46**, 4161–4168 (1992).
 - [122] Emanuele Berti and Nikolaos Stergioulas, “Approximate matching of analytic and numerical solutions for rapidly rotating neutron stars,” *Monthly Notices of the Royal Astronomical Society* **350**, 1416–1430 (2004).
 - [123] Gregory B. Cook, Stuart L. Shapiro, and Saul A. Teukolsky, “Rapidly Rotating Neutron Stars in General Relativity: Realistic Equations of State,” *Astrophys. J.* **424**, 823 (1994).
 - [124] Michi Bauböck, Emanuele Berti, Dimitrios Psaltis, and Feryal Özel, “Relations between neutron-star parameters in the hartle-thorne approximation,” *The Astrophysical Journal* **777**, 68 (2013).
 - [125] M. A. Alpar, A. F. Cheng, M. A. Ruderman, and J. Shaham, “A new class of radio pulsars,” *Nature (London)* **300**, 728–730 (1982).
 - [126] Jason W. T. Hessels, Scott M. Ransom, Ingrid H. Stairs, Paulo C. C. Freire, Victoria M. Kaspi, and Fernando Camilo, “A Radio Pulsar Spinning at 716 Hz,” *Science* **311**, 1901–1904 (2006), arXiv:astro-ph/0601337 [astro-ph].
 - [127] Shen-Shi Du, Xiao-Jin Liu, Zu-Cheng Chen, Zhi-Qiang You, Xing-Jiang Zhu, and Zong-Hong Zhu, “On the initial spin period distribution of neutron stars,” *The Astrophysical Journal* **968**, 105 (2024).
 - [128] Riccardo Gonzo and Canxin Shi, “Boundary to bound dictionary for generic kerr orbits,” *Physical Review D* **108** (2023), 10.1103/physrevd.108.084065.
 - [129] Norman K. Glendenning, ed., *Compact stars : nuclear physics* (2000).
 - [130] L. D. Landau and E. M. Lifshitz, *Mechanics, Third Edition: Volume 1 (Course of Theoretical Physics)*, 3rd ed. (Butterworth-Heinemann, 1976).
 - [131] Richard C. Tolman, “Static solutions of einstein’s field equations for spheres of fluid,” *Phys. Rev.* **55**, 364–373 (1939).
 - [132] Norman K. Glendenning and Christiane Kettner, “Possible third family of compact stars more dense than neutron stars,” *AAP* **353**, L9–L12 (2000), arXiv:astro-ph/9807155 [astro-ph].
 - [133] S. Goriely, N. Chamel, and J. M. Pearson, “Further explorations of skyrme-hartree-fock-bogoliubov mass formulas. xii. stiffness and stability of neutron-star matter,” *Physical Review C* **82** (2010), 10.1103/physrevc.82.035804.
 - [134] Mark Alford, Matt Braby, Mark Paris, and Sanjay Reddy, “Hybrid stars that masquerade as neutron stars,” *The Astrophysical Journal* **629**, 969–978 (2005).
 - [135] L. Engvik, E. Osnes, M. Hjorth-Jensen, G. Bao, and E. Ostgaard, “Asymmetric Nuclear Matter and Neutron Star Properties,” *Astrophys. J.* **469**, 794 (1996), arXiv:nucl-th/9509016 [nucl-th].
 - [136] Lami Suleiman, Morgane Fortin, Julian Leszek Zdunik, and Constança Providência, “Polytropic fits of modern and unified equations of state,” *Physical Review C* **106** (2022), 10.1103/physrevc.106.035805.
 - [137] W. Nazarewicz, J. Dobaczewski, T. R. Werner, J. A. Maruhn, P.-G. Reinhard, K. Rutz, C. R. Chinn, A. S. Umar, and M. R. Strayer, “Structure of proton drip-line nuclei around doubly magic ^{48}Ni ,” *Phys. Rev. C* **53**, 740–751 (1996).
 - [138] P.-G. Reinhard and H. Flocard, “Nuclear effective forces and isotope shifts,” *Nuclear Physics A* **584**, 467–488 (1995).
 - [139] A. Y. Potekhin, A. F. Fantina, N. Chamel, J. M. Pearson, and S. Goriely, “Analytical representations of uni-

- fied equations of state for neutron-star matter,” *Astronomy & Astrophysics* **560**, A48 (2013).
- [140] J. M. Pearson, N. Chamel, S. Goriely, and C. Ducoin, “Inner crust of neutron stars with mass-fitted skyrme functionals,” *Phys. Rev. C* **85**, 065803 (2012).
 - [141] Jocelyn S. Read, Benjamin D. Lackey, Benjamin J. Owen, and John L. Friedman, “Constraints on a phenomenologically parametrized neutron-star equation of state,” *Physical Review D* **79** (2009), 10.1103/physrevd.79.124032.
 - [142] Travis Robson, Neil J Cornish, and Chang Liu, “The construction and use of lisa sensitivity curves,” *Classical and Quantum Gravity* **36**, 105011 (2019).
 - [143] Edward Higson, Will Handley, Michael Hobson, and Anthony Lasenby, “Dynamic nested sampling: an improved algorithm for parameter estimation and evidence calculation,” *Statistics and Computing* **29**, 891–913 (2018).
 - [144] John Skilling, “Nested Sampling,” in *Bayesian Inference and Maximum Entropy Methods in Science and Engineering: 24th International Workshop on Bayesian Inference and Maximum Entropy Methods in Science and Engineering*, American Institute of Physics Conference Series, Vol. 735, edited by Rainer Fischer, Roland Preuss, and Udo Von Toussaint (AIP, 2004) pp. 395–405.
 - [145] John Skilling, “Nested sampling for general Bayesian computation,” *Bayesian Analysis* **1**, 833 – 859 (2006).
 - [146] Joshua S. Speagle, “DYNESTY: a dynamic nested sampling package for estimating Bayesian posteriors and evidences,” *MNRAS* **493**, 3132–3158 (2020), [arXiv:1904.02180 \[astro-ph.IM\]](#).
 - [147] Sergey Kopev, Josh Speagle, Kyle Barbary, Gregory Ashton, Ed Bennett, Johannes Buchner, Carl Schefler, Colm Talbot, Ben Cook, James Guillochon, Patri- cio Cubillos, Andrés Asensio Ramos, Matthieu Darti- aillh, Ilya, Erik Tollerud, Dustin Lang, Ben Johnson, jtmendel, Edward Higson, Thomas Vandal, Tansu Day- lan, Ruth Angus, patelR, Phillip Cargile, Patrick Shee- han, Matt Pitkin, Matthew Kirk, Lu Xu, Joel Leja, and joesuntz, “[joshspeagle/dynesty: v3.0.0](#),” (2025).
 - [148] Philippa S. Cole, James Alvey, Lorenzo Speri, Christoph Weniger, Uddipta Bhardwaj, Davide Gerosa, and Gianfranco Bertone, “[Sequential simulation-based inference for extreme mass ratio inspirals](#),” (2025), [arXiv:2505.16795 \[gr-qc\]](#).
 - [149] Diganta Bandopadhyay and Christopher J. Moore, “Lisa stellar-mass black hole searches with semicoher- ent and particle-swarm methods,” *Phys. Rev. D* **108**, 084014 (2023).
 - [150] Yi Shuen C. Lee, Margaret Millhouse, and Andrew Melatos, “Enhancing the gravitational-wave burst de- tection confidence in expanded detector networks with the bayeswave pipeline,” *Phys. Rev. D* **103**, 062002 (2021).
 - [151] Neil Cornish, Laura Sampson, Nicolás Yunes, and Frans Pretorius, “Gravitational wave tests of general rela- tivity with the parameterized post-einsteinian frame- work,” *Physical Review D* **84** (2011), 10.1103/phys- revd.84.062003.
 - [152] Ambrish M. Raghoonundun and David W. Hobill, “Possible physical realizations of the tolmán vii so- lution,” *Physical Review D* **92** (2015), 10.1103/phys- revd.92.124005.
 - [153] Nan Jiang and Kent Yagi, “Improved analytic modeling of neutron star interiors,” *Physical Review D* **99** (2019), 10.1103/physrevd.99.124029.